Journal of Power Sources 273 (2015) 823–830

Contents lists available at ScienceDirect

Journal of Power Sources

journal homepage: www.elsevier.com/locate/jpowsour

A high power density miniaturized microbial fuel cell having carbon nanotube anodes

Hao Ren [a, *], Soonjae Pyo [b], Jae-Ik Lee [b], Tae-Jin Park [c], Forrest S. Gittleson [d], Frederick C.C. Leung [c], Jongbaeg Kim [b], André D. Taylor [d], Hyung-Sool Lee [e], Junseok Chae [a]

[a] School of Electrical, Computer, and Energy Engineering, Arizona State University, USA
[b] Department of Mechanical Engineering, Yonsei University, Republic of Korea
[c] School of Biological Sciences, The University of Hong Kong, China
[d] Department of Chemical & Environmental Engineering, Yale University, USA
[e] Department of Civil and Environmental Engineering, University of Waterloo, Canada

HIGHLIGHTS

- Miniaturized MFCs with three CNT-based anodes show high power density of 3320 W m^{-3}.
- Biofilm morphology on the anodes are studied and correlated with performance of MFCs.
- High CE and energy conversion efficiency of 69.8% and 22.7% are achieved.
- Power density and efficiencies are high compared with prior art of miniaturized MFCs.
- This research has potential to guide future MFC research with nanostructured electrode.

GRAPHICAL ABSTRACT

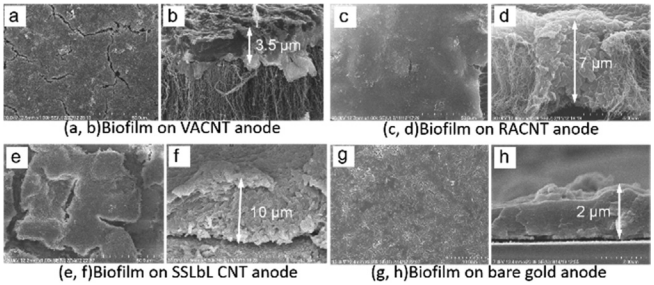

ARTICLE INFO

Article history:
Received 30 June 2014
Received in revised form
10 September 2014
Accepted 25 September 2014
Available online 2 October 2014

Keywords:
Carbon nanotube
Microbial fuel cell
Layer-by-Layer assembly
Surface area to volume ratio (SAV)

ABSTRACT

Microbial fuel cells (MFCs) are a promising technology capable of directly converting the abundant biomass on the planet into electricity. Prior studies have adopted a variety of nanostructured materials with high surface area to volume ratio (SAV), yet the current and power density of these nanostructured materials do not deliver a significant leap over conventional MFCs. This study presents a novel approach to implement a miniaturized MFC with a high SAV of 4000 m^{-1} using three different CNT-based electrode materials: Vertically Aligned CNT (VACNT), Randomly Aligned CNT (RACNT), and Spin-Spray Layer-by-Layer (SSLbL) CNT. These CNT-based electrodes show unique biofilm morphology and thickness. The study of performance parameters of miniaturized MFCs with these CNT-electrodes are conducted with respect to a control bare gold electrode. The results show that CNT-based materials attract more exoelectrogens, *Geobacter* sp., than bare gold, yielding thicker biofilm formation. Among CNT-based electrodes, low sheet resistance electrodes result in thick biofilm generation and high current/power density. The miniaturized MFC having an SSLbL CNT anode exhibits a high volumetric power density of 3320 W m^{-3}. This research may help lay the foundation for future research involving the optimization of MFCS with 2D and 3D nanostructured electrodes.

* Corresponding author. 650 E. Tyler Mall, GWC 302, Tempe, AZ 85281, USA. Tel.: +1 480 374 0122; fax: +1 480 965 0616.
E-mail addresses: hren12@asu.edu, haoren.ustc@gmail.com (H. Ren).

http://dx.doi.org/10.1016/j.jpowsour.2014.09.165
0378-7753/

1. Introduction

Amidst global warming and the negative implications of energy from fossil fuels, there has been significant interest in the development of sustainable energy sources [1]. Bioenergy could potentially constitute a large part of the renewable energy portfolio, provided that the Earth's abundant biomass can be economically converted [2]. Unlike conventional biomass energy conversion techniques, a microbial fuel cell (MFC) is an electrochemical fuel cell that directly converts chemical energy of organic compounds to electrical energy through catalytic reactions of specific microbes called exoelectrogens or anode-respiring bacteria [3–5]. This direct conversion process allows electricity to be generated without intermediate products or equipment, and benefits MFCs' high energy conversion efficiency. During the past few decades, various types of MFCs have been reported in applications for wastewater treatment and renewable energy production [6–10], bioremediation of toxic components [11,12], and power supplies for remote sensors in hazardous or environmentally unfriendly conditions [13].

Researchers have adopted different materials-such as carbon cloth, carbon mesh, graphite rod, felt, foam, fiber brush, reticulated vitreous carbon, tungsten carbide powder, *etc*., which have a high surface area to volume ratio (SAV) as well as mechanical and electrochemical stability [14–19]. Recent research has been focusing on implementing 2D and 3D nanostructured materials with high SAV such as carbon nanotubes (CNT) and graphene. CNT and graphene are two nanostructured carbon allotropes, which are attractive materials due to their high SAV, high conductivity, excellent electrochemical characteristics, superb mechanical and chemical stability, and manufacturing compatibility with batch-mode microfabrication [20–23]. Both CNTs and graphene have been used as 2D and 3D carbon based anode materials for MFCs, such as in graphene sponge [24], reduced graphene oxide on carbon fiber [25], CNT/polyaniline or CNT/chitosan composite [26,27], multi-walled CNT [28–30], polyaniline hybridized graphene [31], chitosan/vacuum-stripped graphene scaffold [32], 3D graphene on Ni foam [33,34], and reduced graphene oxide/CNT coated scaffold [35], yielding a SAV as high as 20,000 m^{-1}; however, the reported maximum areal power density ranges from 19 mW m^{-2} to 1.57 W m^{-2}. Based on projected electrode area, the volumetric power density ranges from 6.3 W m^{-3} to 392 W m^{-3} [24,29,36], which still does not deliver a significant leap over conventional MFCs. Moreover, the biocompatibility of CNTs remains questionable [37] and some prior studies of CNT-based MFCs show lower performance than MFCs having anodes of conventional carbon-based materials [26,28,38,39]. Besides implementing high SAV materials as anode, the cathode impacts the performance of MFCs significantly as well - especially air-cathode MFCs [40]. CNTs and graphene based materials have also been used as cathodes materials in air-cathode MFCs, of which the cathode becomes the bottleneck, as reported by Wang et al. 2011 and Khilari et al. 2013 [41,42].

Miniaturized MFCs reduce the characteristic length scales of MFCs to the micrometer range, which results in chamber volumes which are on the μL scale [36,43–47]. In this work, we report the formation and morphology of biofilm on three different CNT-based electrode materials, and correlate the biofilm formation and morphology to the characteristics of the miniaturized MFC, including coulombic efficiency and areal/volumetric power density. The three types of anodes using CNT materials with different sheet resistance and morphology are: (1) Vertically Aligned Carbon Nanotubes (VACNT), (2) Randomly Aligned Carbon Nanotubes (RACNT), and (3) Spin-Spray Layer-by-Layer Carbon Nanotubes (SSLbL CNT).

2. Experimental

2.1. Bare gold electrode

The bare gold electrodes were deposited on a glass slide (micro slides, 4.6 × 2.6 × 0.1 cm^3, VWR) with six through holes pre-drilled mechanically (12 inch Bench Drill, Model 315.219140, Craftsman): one inlet, one outlet, and four for assembly (Fig. S1(a)). Afterward, Cr/Au (20 nm/200 nm) films were deposited on the glass slides via sputtering on the glass slides (Emitech K675XD Turbo Sputter Coater) (Fig. S1(b)). We chose a bare gold anode as control, following prior work that reported little difference exists on the attraction of *Geobacter* on carbon based material and gold [48].

2.2. VACNT and RACNT

The VACNTs were directly synthesized on a quartz slide (quartz microscope slide, 5.08 × 2.54 × 0.1 cm^3, Alfa Aesar) by catalytic chemical vapor deposition (CVD) (Fig. S1(e)) [49]. After 5 nm-thick iron (Fe) catalysts were deposited on the quartz slide by electron-beam evaporation, the quartz slide was placed into a growth chamber. The temperature and pressure for CNT synthesis was 700 °C and 4 Torr, respectively. When the growth conditions were stabilized, the chamber was purged with nitrogen (N_2) gas of 10 sccm. The CNTs were then grown under acetylene (C_2H_2) ambience after ammonia (NH_3) pretreatment for 30 min. The NH_3 pretreatment is necessary for the vertical alignment of CNTs [50]. In contrast to the synthesis of VACNTs, RACNTs were synthesized without NH_3 pretreatment. VACNT shows highly directional CNT growth due to strong van der Waals interaction between densely grown CNTs. NH_3 prevents Fe catalysts from being covered by amorphous carbon during synthesis, resulting in a high density of nucleation sites for CNTs growth. Without NH_3 pretreatment, curved and randomly oriented CNTs are synthesized and amorphous carbon is found between the CNTs.

2.3. SSLbL CNT

The SSLbL apparatus and experimental procedure for assembling polymer-CNT nano-composite films has been described previously [51]. Briefly, the SSLbL apparatus allows the sequential spraying of polyelectrolyte solutions and the rinsing of water onto a horizontal rotating substrate using three vertically-oriented sprayers and a spin-coater. For SSLbL anode films, an aqueous solution of 1% poly(styrene sulfonate) with 0.5 mg mL^{-1} multi-walled carbon nanotubes was prepared with three hours of bath sonication followed by 45 min of tip sonication and 1.5 h of centrifugation at 3000 rpm to produce a stable dispersion. A solution of 10-mM poly(vinyl alcohol) at a pH of 2.8 was used as the polycation. Bare gold-coated glass slides were mounted onto the SSLbL vacuum chuck and rotated at 3000 rpm while solutions and rinse water were sprayed. A single bilayer was assembled using a spray/dry procedure of polycation, rinse, dry, polyanion, rinse, and dry. Deionized water matching the pH of the polycation solution was used for the rinse. Between bilayers, the substrate was dried at approximately 45 °C for 4 s. The multi-walled carbon nanotubes used in SSLbL CNT electrodes have a median diameter of 6.6 nm and an aspect ratio ~1000.

2.4. Inoculum

The inoculum for the micro-scale MFC was obtained from an acetate-fed microbial electrolysis cell (MEC), which had a *Geobacter*-enriched bacterial community originally from anaerobic-digestion sludge. The anolyte was composed of a 25-mM sodium

acetate medium with 1680 mg KH_2PO_4, 12,400 mg Na_2HPO_4, 1600 mg NaCl, 380 mg NH_4Cl, 5 mg EDTA, 30 mg $MgSO_4{\cdot}7H_2O$, 5 mg $MnSO_4{\cdot}H_2O$, 10 mg NaCl, 1 mg $Co(NO_3)_2$, 1 mg $CaCl_2$, 0.001 mg $ZnSO_4{\cdot}7H_2O$, 0.001 mg $ZnSO_4{\cdot}7H_2O$, 0.1 mg $CuSO_4{\cdot}5H_2O$, 0.1 mg $AlK(SO_4)_2$, 0.1 mg H_3BO_3, 0.1 mg $Na_2MoO_4{\cdot}2H_2O$, 0.1 mg Na_2SeO_3, 0.1 mg $Na_2WO_4{\cdot}2H_2O$, 0.2 mg $NiCl_2{\cdot}6H_2O$, and 1 mg $FeSO_4{\cdot}7H_2O$ (per liter of deionized water) (pH 7.8 ± 0.2). For the start-up process, inoculum and anolyte were mixed at a volumetric ratio of 1:1. The catholyte was composed of 100-mM potassium ferricyanide in a 100-mM phosphate buffer solution (pH 7.4). The anolyte and catholyte were supplied into the micro-scale MFC using a syringe pump. The MFCs operated at 30 °C.

2.5. Start-up and data acquisition

Anolyte/catholyte solutions were pumped into the corresponding chambers at a flow rate of 0.25 μL min^{-1}. It typically takes 5–7 days to form a mature biofilm (Fig. S3). Once the start-up process completes, the output current begins to reach steady state.

The current generated by the MFCs was recorded every minute by measuring voltage drop across an external resistor connected between the anode and the cathode using a data acquisition system (DAQ/68, National Instrument). During start-up, the MFCs were operated at 0.25 μL min^{-1} and the external resistor was set to 148-Ω. Once the start-up process completed, the flow rate was increased and polarization measurement was performed. For the polarization curve measurement, a series of resistors was employed, ranging from 148 Ω to 932 kΩ.

2.6. Coulombic efficiency (CE) and energy conversion efficiency measurement

Coulombic efficiency and energy conversion efficiency were measured by stopping the anolyte supply while keeping the catholyte supply; the current over time domain was monitored while the catholyte kept flowing. Coulombic efficiency is the ratio of total coulombs transferred to the anode from the substrate to the maximum possible coulombs transferred if all substrate removal produced current. That is, $CE = C_P/C_T \times 100\%$, where C_P is the total coulombs calculated by integrating the current over the time for substrate consumption and C_T is the maximum possible coulombs of the substrate $C_T = V \times b \times A \times e \times (mol_{substrate})$. V is the volume of anode chamber (m^3), b is the number of moles of electrons produced by oxidation of substrate ($b = 8$ mol e^-/mol acetate), A is Avogadro's number (6.023×10^{23} molecules/mol), e is the electron charge (1.6×10^{-19}C/electron), and $mol_{substrate}$ is the moles of acetate oxidized. The CE measurement of VACNT, RACNT and bare gold anode is illustrated in Fig. S4 (CE of SSLbL CNT is shown in Fig. 4).

Energy conversion efficiency is the ratio of total energy harvested by the MFC to the maximum possible energy that the biomass can produce (standard molar enthalpy of biomass): $\eta = E_P/E_T \times 100\%$, where E_P is the total energy calculated by integrating the power output over the time for substrate consumption and E_T is the maximum possible energy of the biomass $E_T = V \times c \times \Delta_f H^\circ$. V is the volume of the anode chamber (m^3), c is the concentration of biomass in the anode chamber ($c = 25$ mol m^{-3}, sodium acetate), and $\Delta_f H^\circ$ is the standard molar enthalpy of formation (708.8 kJ mol^{-1} for sodium acetate).

3. Results and discussion

3.1. Biofilm morphology and thickness on three CNT-based anodes

Fig. 1 shows the SEM images of the three CNT-based materials. Sheet resistance of the anodes was measured by a four-point probe method. The sheet resistance of VACNT, RACNT, SSLbL CNT, and bare gold electrodes were measured to be $1.48 \pm 0.004 \times 10^3$, $2.98 \pm 0.354 \times 10^3$, $3.84 \pm 0.17 \times 10^0$, and $3.68 \pm 0.07 \times 10^0$ Ω $square^{-1}$ respectively. VACNT and RACNT electrodes have substantially higher sheet resistance than those of SSLbL CNT and bare gold electrodes.

Ex-situ characterization of morphology and thickness of biofilm on the CNT-based anodes were performed by scanning electron microscopy (SEM) as shown in Fig. 2 (procedure of biofilm fixation is shown in Supplementary materials). VACNT, RACNT, SSLbL CNT and bare gold anodes have biofilms thicknesses of approximately 3.3 ± 0.2 μm, 6.5 ± 0.5 μm, 9.0 ± 1.0 μm and 1.8 ± 0.2 μm respectively (Fig. 2(a)–(h)). The bare gold anode, despite having very low sheet resistance, has a biofilm considerably thinner than others, suggesting CNTs attract more exoelectrogens.

16S rRNA analysis was performed to find the microbial community diversity and structures, as illustrated in Figs. S5, S6 and Table S1 (experimental procedures in Supplementary materials). The results reveal that the *Geobacter* species dominate the biofilm, comprising 40.8% of the total biofilm. The remainder of the biofilm is made up of unclassified bacterial species, such as *Brucellaceae, Actinomycetales*, etc. The observed phylogenetic diversity likely reflects syntrophic interactions between exoelectrogens and non-exoelectrogens [52].

The biofilm morphology and thickness characterization suggests that CNT-based materials attract more exoelectrogens to form thicker biofilms than does bare gold. Prior study reports that cell growth is significantly accelerated on a nanostructured material-TiO_2 nanotube [53]. Although the promotion mechanisms of the nanostructured material on cell proliferation are still not fully understood [54], it is plausible that the thicker biofilm generation may be due to the nanostructured CNTs, which provide a larger surface area for *Geobacter* sp: cell adhesion. The thicker biofilm on the CNT-based anodes also implies the biocompatibility of the CNT-based materials with *Geobacter* sp. The previous study by Ren et al. 2011 reported a discrepancy between the microbial and electrochemical responses on the anode, yet our results suggest an indirect link between the thickness of the biofilm and current and power generation capability [55].

Of the three CNT-based anodes, the SSLbL CNT has a lowest sheet resistance of $3.84 \pm 0.17 \times 10^0$ Ω $square^{-1}$, (significantly lower than those of VACNT and RACNT,~10^3 Ω $square^{-1}$), and the thickest (9.0 ± 1.0 μm) biofilm, suggesting the sheet resistance of the anode impacts the biofilm thickness. Xie et al. has shown that a graphene sponge sandwiched by a stainless-steel current collector produces significantly higher current than a bare graphene sponge anode. Here the stainless-steel electrode has a lower resistance than the graphene sponge, providing a “highway” for electrons [24]. This work suggests that the high electrode resistance (graphene sponge itself, ~180 Ω) limits the current production from *Shewanella* MR1. The sheet resistance of the VACNT and RACNT anodes are $1.48 \pm 0.004 \times 10^3$, and $2.98 \pm 0.354 \times 10^3$ Ω $square^{-1}$ respectively, which are on the same order of internal resistance of MFCs having them as anodes, 4.3 ± 0.03 kΩ and 2.3 ± 0.08 kΩ respectively. The high sheet resistance of VACNT and RACNT electrodes likely limits the current from exoelectrogens. The SSLbL CNT anode possesses relatively high surface area and low sheet resistance, which result in the thickest biofilm. The measured data, however, does not provide conclusive evidence as to which aspect of features impact biofilm formation most extremely.

3.2. Current/power density and efficiency of miniaturized MFCs

A miniaturized MFC having an SAV of 4000 m^{-1} is illustrated in Figs. S1–S3. The current/power density of miniaturized MFCs that

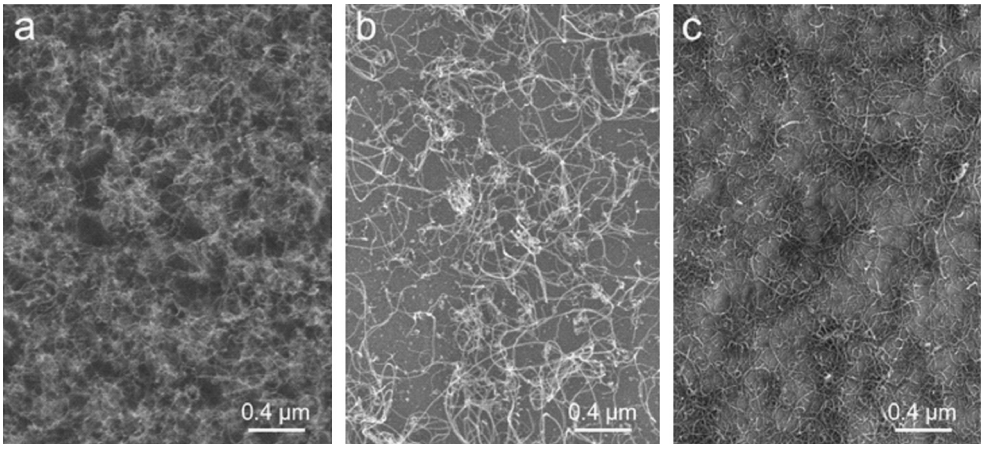

Fig. 1. SEM images of three types of CNT based anodes: (a) VACNT, (b) RACNT, and (c) SSLbL (scale bar: 400 nm).

have CNT-based anodes was characterized via polarization curves (Fig. 3) and the operating data for these curves is shown in Fig. S7. The flow rate of anolyte/catholyte was set to be 2 μL min^{-1}. All MFCs show 0.7–0.8 V open circuit voltage, suggesting oxygen intrusion is successfully mitigated. The maximum current and power densities of 2.59 ± 0.01 A m^{-2} and 0.83 ± 0.01 W m^{-2}, respectively, were obtained from the SSLbL CNT MFC, in accordance with the biofilm thickness measurements (Fig. 2). Maximum volumetric power density of 3320 ± 40 W m^{-3} was obtained by the SSLbL CNT MFC, the highest among all MFCs.

Fig. 4 shows the transient current profile to measure CE and energy conversion efficiency of the SSLbL CNT MFC. The anolyte flow was stopped, while keeping the catholyte running to measure harvested charges from the anolyte in the anode chamber [56] A high CE of 69.8% and an energy conversion efficiency of 22.7% were achieved (calculation of CE and EE from Fig. 4 is shown in Supplementary materials). CEs of 61.3%, 73%, 80.9% were also achieved for the VACNT, RACNT, and bare gold anodes, respectively (Fig. S4).

3.3. Correlation between biofilm and current/power density

A schematic illustration of the biofilm formation on three types of CNT-based and bare gold anodes is shown in Fig. 5. The high density and vertical structure of VACNT prohibits exoelectrogens from placing themselves inside the VACNT forest, resulting in a thin biofilm and low current/power density. In contrast, RACNT film offers rather porous features and thus can accommodate exoelectrogens between CNTs, resulting in a thick biofilm. The SSLbL CNT film is composed of horizontally oriented CNTs conjugated with polymers. A stratified-rod-network model of the electrical conductance of these SSLBL films can be found in a previous study [57]. Here we show that this structure results in the thickest exoelectrogen biofilm while the bare gold control anode has the thinnest biofilm.

The schematic illustration matches well with experimental observation. VACNT and RACNT electrodes show similar sheet resistances, yet the RACNT anode forms a thicker biofilm and yields a higher current/power density than the VACNT films. The RACNT film may allow exoelectrogens to penetrate between the individual CNTs whereas exoelectrogens cannot penetrate inside the dense VACNT forest (Fig. 2(a)–(d)). Exoelectrogens, similar to cells, generate mechanical force for adhesion on electrodes [58]. The dense VACNT forest may resist the bending of CNTs and thus exoelectrogens cannot penetrate. Prior studies by Ren et al. 2011 and Lyon et al. 2010 report the external loads impact not only current/power density but also the biofilm architecture and bacterial communities. Higher external resistance (5–10 kΩ) results in a lower current/power density as well as a lower cell count [59,60]. Our finding aligns well with these prior studies with regards to parameters that impact the biofilm structure, including materials and sheet resistance of anode.

The electron generation capability of the SSLbL CNT biofilm is estimated to be 4.22 × 10^5 electrons/s, as shown in the SI. This calculation is similar to that of *Shewanella MR1*, which can generate 10^6 electrons s^{-1} [61]. This calculation supports the postulation that the electron generation rate and exoelectrogen population have a major impact on the performance of MFCs. Porous electrodes were reported to enhance the mass transfer of acetate and H^+ carrying buffer, aiding the electron generation capability of *Geobacter* sp. deep inside the biofilm [31,32]. Therefore, anode materials having high surface-area-to-volume ratio, high porosity, and high biocompatibility (resulting in a large exoelectrogen population) help to reduce areal resistivity, consequently improving current/power density.

3.4. Discussion on the impact of the resistivity of the anode

Energy loss in micro-scale MFCs involves two parts, ohmic loss and overpotential. The ohmic loss can be measured using the slope of the ohmic region in polarization curves, while the total overpotential is composed of overpotentials at the anode, cathode, and overpotential induced by the existence of a pH discrepancy between the anode and cathode chambers, etc [6,7,43,62–64].

The areal resistivity may be used to obtain the ohmic loss. Areal resistivity can be computed as:

$$r_i = r_a + r_c + r_m + r_e \quad (1)$$

where r_i is the total areal resistivity and r_a, r_c, r_m, r_e are areal resistivity of anode, cathode, ion exchange membrane, and electrolyte, respectively. r_a is composed of the resistance of the anode itself and electron generation/transfer from exoelectrogens to the anode. r_c involves the resistance of the cathode itself, potassium ferricyanide ion transfer from the bulk solution to the vicinity of the cathode and reduction of the ions at the cathode. r_m is mainly determined by the resistivity of the ion exchange membrane for movement of counter ions (protons, or other cations in acetate medium) across the membrane. r_e is a function of the distance between the two electrodes and the conductivity of the acetate medium (electrolyte):

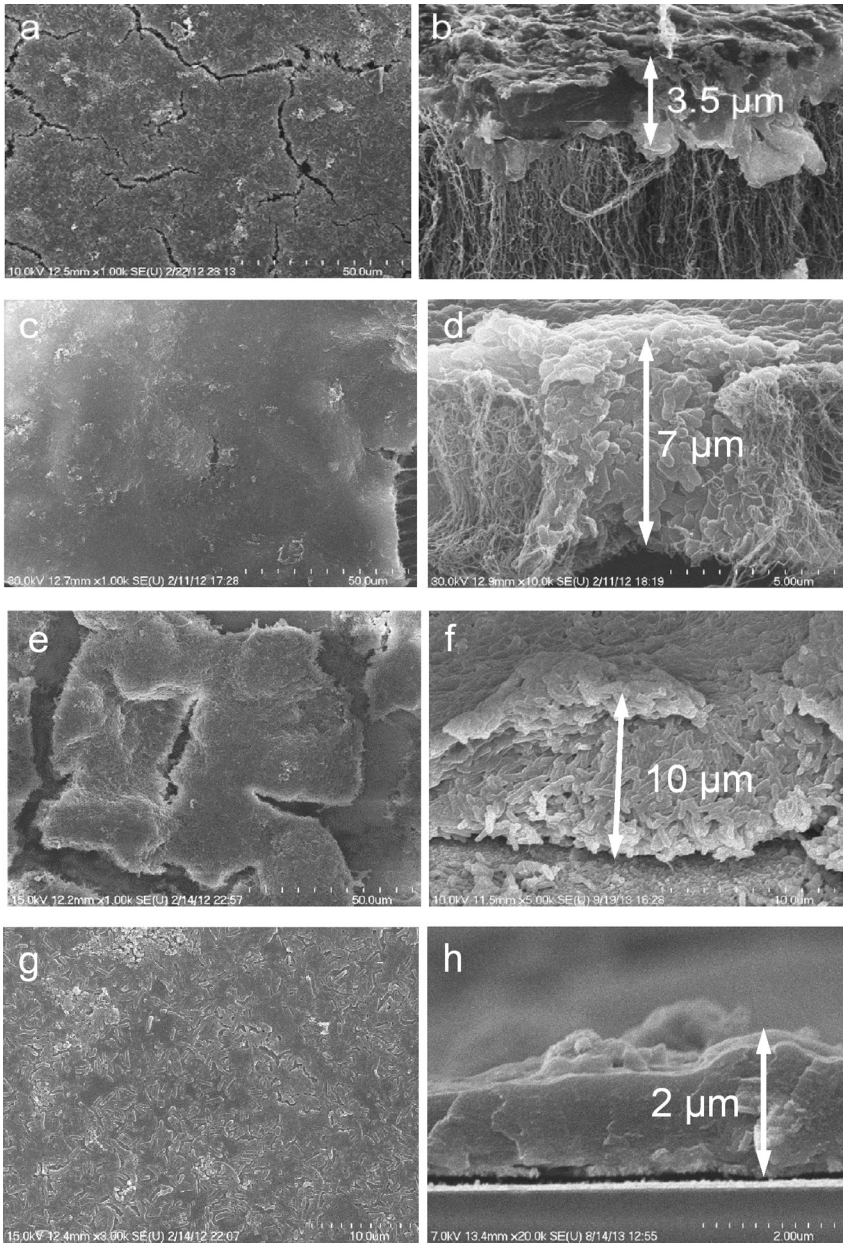

Fig. 2. Top and cross-sectional view SEM images of (a, b) VACNT anode, (c, d) RACNT anode, (e, f) SSLbL CNT anode, and (g, h) bare gold anode: The thickness of biofilm of these anodes are 3.3 ± 0.2 μm, 6.5 ± 0.5 μm, 9 ± 1 μm and 1.8 ± 0.2 μm thick, respectively (the figures show the thickest part), suggesting CNT-based anodes attract more exoelectrogen than the gold anode to form thick biofilm. (d) Shows the exoelectrogen and RACNT weaves together well, suggesting high biocompatibility of RACNT.

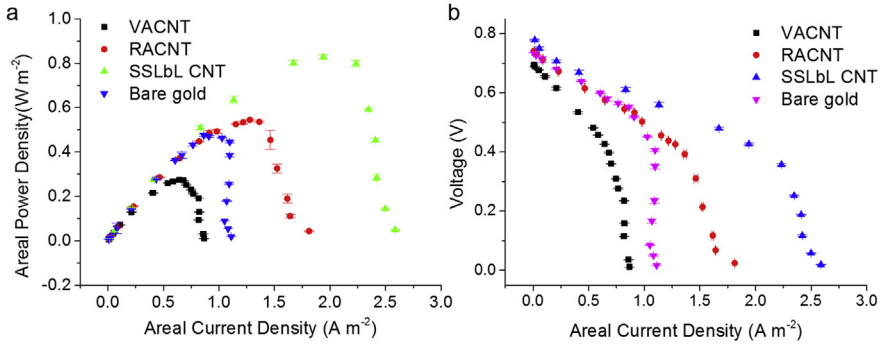

Fig. 3. Polarization curves of miniaturized MFCs with CNT-based and gold anodes: (a) Power density versus current density and (b) voltage versus current density. The measured current is assumed to be solely from oxidizing acetate in the anolyte [3,73,74].

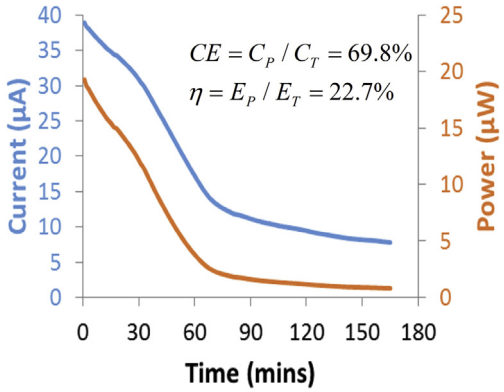

Fig. 4. Current and power versus run time in the MFC with SSLbL CNT anode for Coulombic efficiency (CE) and energy conversion efficiency measurement. The calculated CE and energy conversion efficiency are 69.8% and 22.7%, respectively.

$$r_e = \frac{l}{K} \quad (2)$$

where l is the distance between the two electrodes, and K is the specific conductivity of the electrolyte.

The distance between anode and cathode (l) is the sum of the thicknesses of the two gaskets, 500 μm total, and ion exchange membrane, 178 μm, for a total distance of 678 μm. The specific conductivity (K) of the anolyte and catholyte were measured as 5.7 mS cm^{-1} and 2.5 mS cm^{-1}, respectively. Based on these measured and given parameters, r_e is equal to 14.4 Ω cm^2 r_m, the resistivity of the ion exchange membrane (Nafion 117), was measured to be 10 Ω cm^2, in phosphate buffer medium. r_c, the resistivity of the cathode, is also low, in the magnitude of 10 Ω cm^2. As a result, r_a, the anode resistivity, is responsible for the majority of total areal resistivity.

Of r_a, the areal resistivity of the anode, the resistivity of the anode material itself is negligible for the SSLbL CNT and bare gold, and therefore the majority of the areal resistivity is attributed to the resistance of electron generation by exoelectrogen metabolism and transfer from exoelectrogens to anode. On the other hand, the VACNT and RACNT anodes have high sheet resistance, which significantly adds to the anode resistivity. This limits current/power density. Fig. 3 shows that all MFCs suffer from concentration loss at high current density. This concentration loss is believed to be associated with the limited extracellular electron transfer (EET) at high current density [65] and a mass transfer limitation of the transfer of acetate and H^+ carrying buffer from bulk to biofilm.

Table 1
Measured specifications of 4 different anodes in miniaturized MFCs.

	Sheet resistance [ohm $square^{-1}$]	Areal resistivity [kΩ cm^2]	Biofilm thickness [μm]	Current density [A m^{-2}]	Power density [W m^{-2}]
VACNT	$1.48 \pm 0.004 \times 10^3$	4.3 ± 0.03	3.3 ± 0.2	0.87 ± 0.001	0.27 ± 0.001
RACNT	$2.98 \pm 0.354 \times 10^3$	2.3 ± 0.08	6.5 ± 0.5	1.81 ± 0.005	0.54 ± 0.004
SSLbL CNT	$3.84 \pm 0.17 \times 10^0$	1.2 ± 0.03	9.0 ± 1.0	2.59 ± 0.010	0.83 ± 0.010
Bare gold	$3.68 \pm 0.07 \times 10^0$	2.2 ± 0.12	1.8 ± 0.2	1.11 ± 0.002	0.48 ± 0.006

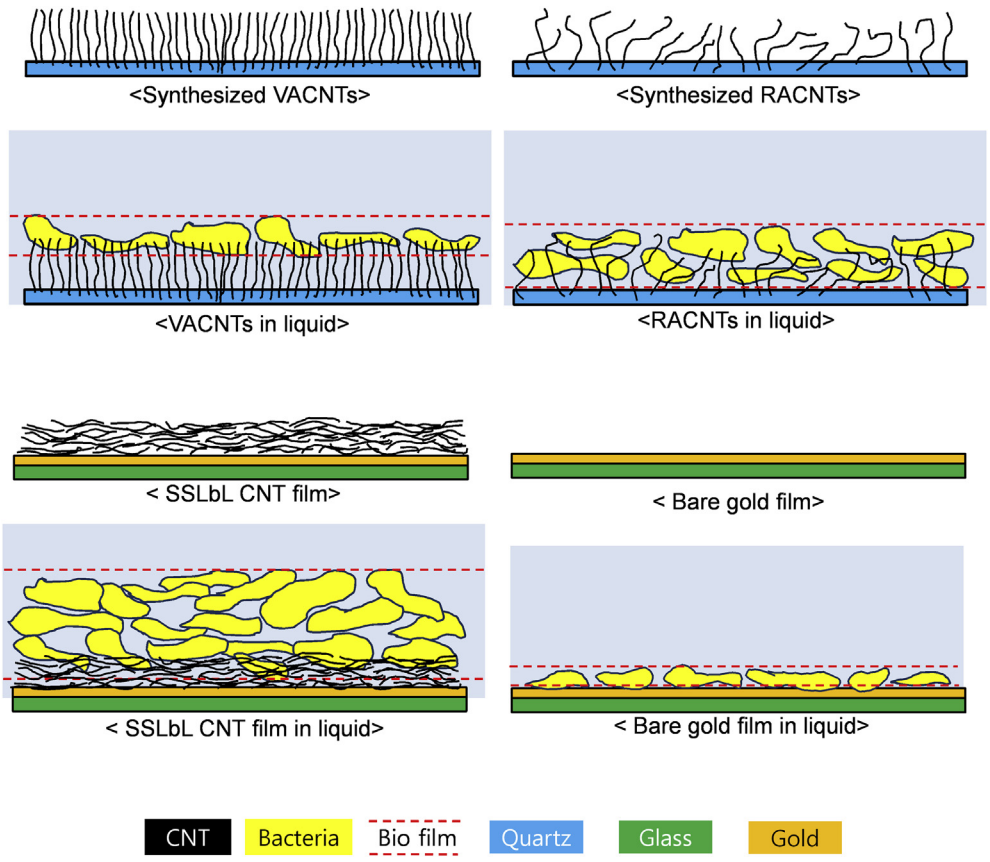

Fig. 5. Schematic illustration of three types of CNT-based anodes: (a) VACNT (Vertically Aligned Carbon Nanotubes), (b) RACNT (Randomly Aligned Carbon Nanotubes), (c) SSLbL (Spin-Spray Layer-by-Layer Carbon Nanotubes) and (d) bare gold anode. *Geobacter* sp. form their biofilm on those anodes and the thickness of the biofilm is a function of types of anodes.

Table 2
A comparison of specifications of this work compared with prior art (the significance of bold is to highlight this work).

Performance parameters	Mink et al. [36]	Inoue et al. [46]	Choi et al. [56]	Qian et al. [44]	Siu et al. [45]	Biffinger et al. [72]	This work (SSLbL CNT)
Anode material	CNT	CNT	Gold	Gold	Gold	Carbon/Pt ink	**CNT + polymer**
Anode volume [μL]	1.5	40	4.5	1.5	15	25[b]	**12.5**
Anode area [cm^2]	0.25	0.24	2.25	0.15	1.2	0.45	**0.5**
Areal resistivity [$k\Omega \cdot cm^2$]	N/A	N/A	22.5	4.5	30	3.375	**1.2 ± 0.03**
P_{areal} [$W\ m^{-2}$]	0.0196	0.0738	0.047	0.015	0.004	0.06	**0.83 ± 0.01**
$P_{volumetric}$ [$W\ m^{-3}$]	392	343	2333	15.3	4.24[a]	10	**3320 ± 40**
CE [%]	N/A	N/A	31	2.8	14.7	NA	**60%–80%**

[a] Calculated based on the reported data.
[b] The volume of the device.

It is also helpful to compare the performance of miniaturized MFCs with different anodes to provide helpful information for future performance improvement. Because exoelectrogens are the catalysts for current/power generation in MFCs, biofilm morphology/thickness has a significant impact on the current/power generation. On the other hand, anode sheet resistance also impacts current/power generation. High sheet resistance increases the overall internal resistance of MFCs, which in turn limits the current/power generation. Based on biofilm thickness characterization of four types of anodes, the SSLbL CNT anode has the thickest biofilm, at 9.0 ± 1.0 μm, as well as the highest current/power generation capability, shown to be 2.59 ± 0.010 A m^{-2} and 0.83 ± 0.010 W m^{-2} respectively. The RACNT has the second thickest biofilm, 6.5 ± 0.5 μm, and delivers the second highest current/power generation capability, 1.81 ± 0.005 A m^{-2} and 0.54 ± 0.004 W m^{-2}. VACNT anode has the third thickest biofilm, 3.3 ± 0.2 μm, which is thicker than bare gold control at 1.8 ± 0.2 μm, yet had the lowest current/power generation capability, 0.87 ± 0.001 A m^{-2} and 0.27 ± 0.001 W m^{-2}, lower than the bare gold control at 1.11 ± 0.006 A m^{-2} and 0.49 ± 0.002 W m^{-2}. This result implies that the high sheet resistance of VACNT anode degrades current/power generation capability. The measured specifications are summarized in Table 1.

3.5. Comparison with prior work

Table 2 summarizes measured specifications of the SSLbL CNT in comparison to previously reported miniaturized MFCs. Areal and volumetric power densities and the CE of this work are substantially higher than those of prior studies; correspondingly, areal resistivity of this work is much lower than that of prior studies. Miniaturized MFCs using CNT anodes exist, yet their areal and volumetric power density are very low [36,46]. The improvements shown here suggest successful biocompatibility of the CNT materials used in this work.

Fig. 6 and Fig. S9 show the areal power density, volumetric power density and CE of the SSLbL CNT compared to prior studies - including macro/meso-scale and micro-scale MFCs. The volumetric power density of the SSLbL CNT MFC is 3320 ± 40 W m^{-3}. Both the areal power density and CE of this work are also substantially higher than those of most micro-scale MFCs and are comparable with those of macro-/meso-scale MFCs. Most micro-scale MFCs deploying *Geobacter* reported previously used PDMS (Polydimethylsiloxane) as their gaskets, which has substantial oxygen permeability. This results in severe oxygen intrusion into the anode chamber, leading to a very low CE. Our work implemented a silicone gasket, which has an oxygen permeability (19,685 cm^3 mm m^{-2} day^{-1} atm^{-1}), 2.7 times lower than that of PDMS (52,531 cm^3 mm m^{-2} day^{-1} atm^{-1}), which yields a higher CE.

The areal/volumetric power density of 0.83 ± 0.01 W m^{-2} and 3320 ± 40 W m^{-3}, respectively, are comparable or higher than those of other types of renewable energy conversion techniques, such as thermoelectric (0.6 W m^{-2}) [66], piezoelectric (200 W m^{-3}) [67], and indoor photovoltaics (1 W m^{-2}) [68], suggesting that the miniaturized MFC may be an attractive candidate for renewable energy conversion approaches. Approximately 50–80 μW can be generated from the miniaturized MFCs at a voltage of 0.4–0.5 V, which may fit well to sub-100 μW applications such as ultra-low power MCUs (microcontroller units), data storage, passive RFID tags, transmitters for wireless sensor network, implantable medical devices, *etc.* [68–71]. Furthermore, the miniaturized MFCs can be integrated into low-power electronics for autonomous operation in rural and environmentally unfriendly places where stand-alone maintenance and free operation are demanded [19,72].

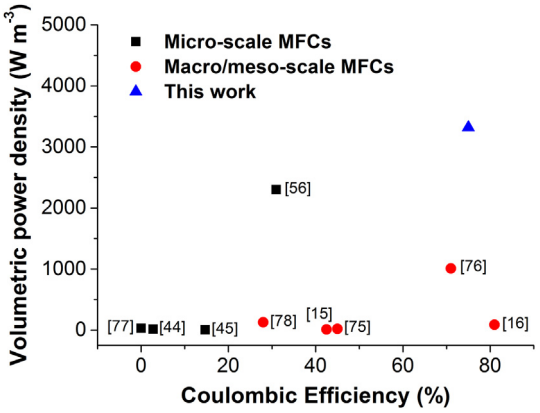

Fig. 6. A comparison of volumetric power density and CE of SSLbL CNT with existing macro-/meso- and micro-scale MFCs [15,16,44,45,56,75–78]; the volumetric power density of this work is higher than all previous MFCs, regardless of scale, and the CE of this work is substantially higher than those of most micro-scale MFCs and is comparable with those of macro-/meso-scale MFCs.

4. Conclusion

We report a miniaturized MFC having a high SAV of 4000 m^{-1} also with a high volumetric power density. Three types of CNT-based anodes with different morphologies and sheet resistances (VACNT, RACNT, and SSLbL CNT, along with a bare gold control) were evaluated using miniaturized MFCs. SEM and polarization curves of miniaturized MFCs having these anodes were used to analyze the morphology and thickness of generated biofilms as well as current/power generation capabilities. All CNT-based anodes form thicker biofilms than the bare gold anode control, with the SSLbL CNT anode having the lowest sheet-resistance of 3.84 ± 0.17 Ω $square^{-1}$, the thickest biofilm of 9 μm, and a current/power density of 2.59 ± 0.01 A m^{-2} and 0.83 ± 0.01 W m^{-2}. We observed distinctly different biofilm morphologies and thicknesses from VACNT and

RACNT anodes, most likely attributable to the morphology of the CNT forest – consequently resulting in two different current/power densities with the VACNT anodes delivering substantially lower current/power densities than RACNT anodes. The highest power density of 3320 ± 40 W m^{-3} was obtained by the SSLbL CNT anode, more than 8.5 times the power densities reported by prior-art MFCs using 2D and 3D nanostructured electrodes. A high CE of 60%–80% supports the use of MFCs for renewable energy conversion in low-power electronics applications.

Appendix A. Supplementary data

Supplementary data related to this article can be found at http://dx.doi.org/10.1016/j.jpowsour.2014.09.165.

References

[1] M.E. Himmel, S.-Y. Ding, D.K. Johnson, W.S. Adney, M.R. Nimlos, J.W. Brady, T.D. Foust, Science 315 (2007) 804–807.
[2] A.J. Ragauskas, C.K. Williams, B.H. Davison, G. Britovsek, J. Cairney, C.A. Eckert, W.J. Frederick, J.P. Hallett, D.J. Leak, C.L. Liotta, Science 311 (2006) 484–489.
[3] D.R. Bond, D.E. Holmes, L.M. Tender, D.R. Lovley, Science 295 (2002) 483–485.
[4] S.K. Chaudhuri, D.R. Lovley, Nat. Biotechnol. 21 (2003) 1229–1232.
[5] B.E. Logan, K. Rabaey, Science 337 (2012) 686–690.
[6] B.E. Logan, B. Hamelers, R. Rozendal, U. Schröder, J. Keller, S. Freguia, P. Aelterman, W. Verstraete, K. Rabaey, Environ. Sci. Technol. 40 (2006) 5181–5192.
[7] K. Rabaey, W. Verstraete, Trends Biotechnol. 23 (2005) 291–298.
[8] B.E. Logan, Appl. Microbiol. Biotechnol. 85 (2010) 1665–1671.
[9] A. ElMekawy, S. Srikanth, K. Vanbroekhoven, H. De Wever, D. Pant, J. Power Sources 262 (2014) 183–191.
[10] D. Pant, D. Arslan, G. Van Bogaert, Y.A. Gallego, H. De Wever, L. Diels, K. Vanbroekhoven, Environ. Technol. 34 (2013) 1935–1945.
[11] K.B. Gregory, D.R. Lovley, Environ. Sci. Technol. 39 (2005) 8943–8947.
[12] L. Lu, T. Huggins, S. Jin, Y. Zuo, Z.J. Ren, Environ. Sci. Technol. 48 (2014) 4021–4029.
[13] L.M. Tender, S.A. Gray, E. Groveman, D.A. Lowy, P. Kauffman, J. Melhado, R.C. Tyce, D. Flynn, R. Petrecca, J. Dobarro, J. Power Sources 179 (2008) 571–575.
[14] B. Logan, Microbial Fuel Cells, John Wiley & Sons, Inc., Hoboken, New Jersey, 2008.
[15] H. Liu, B.E. Logan, Environ. Sci. Technol. 38 (2004) 4040–4046.
[16] K. Rabaey, N. Boon, S.D. Siciliano, M. Verhaege, W. Verstraete, Appl. Environ. Microbiol. 70 (2004) 5373–5382.
[17] Z. He, S.D. Minteer, L.T. Angenent, Environ. Sci. Technol. 39 (2005) 5262–5267.
[18] M. Rosenbaum, F. Zhao, U. Schroder, F. Scholz, Angew. Chem. Int. Ed. 45 (2006) 6658–6661.
[19] B.R. Ringeisen, E. Henderson, P.K. Wu, J. Pietron, R. Ray, B. Little, J.C. Biffinger, J.M. Jones-Meehan, Environ. Sci. Technol. 40 (2006) 2629–2634.
[20] R.H. Baughman, A.A. Zakhidov, W.A. de Heer, Science 297 (2002) 787–792.
[21] S.W. Lee, N. Yabuuchi, B.M. Gallant, S. Chen, B.S. Kim, P.T. Hammond, Y. Shao-Horn, Nat. Nanotechnol. 5 (2010) 531–537.
[22] A.D. Taylor, M. Michel, R.C. Sekol, J.M. Kizuka, N.A. Kotov, L.T. Thompson, Adv. Funct. Mater. 18 (2008) 3003–3009.
[23] A.K. Geim, K.S. Novoselov, Nat. Mater. 6 (2007) 183–191.
[24] X. Xie, G.H. Yu, N. Liu, Z.N. Bao, C.S. Criddle, Y. Cui, Energy & Environ. Sci. 5 (2012) 6862–6866.
[25] L. Xiao, J. Damien, J. Luo, H.D. Jang, J. Huang, Z. He, J. Power Sources 208 (2012) 187–192.
[26] Y. Qiao, C.M. Li, S.J. Bao, Q.L. Bao, J. Power Sources 170 (2007) 79–84.
[27] X.-W. Liu, X.-F. Sun, Y.-X. Huang, G.-P. Sheng, S.-G. Wang, H.-Q. Yu, Energy & Environ. Sci. 4 (2011) 1422–1427.
[28] H.Y. Tsai, C.C. Wu, C.Y. Lee, E.P. Shih, J. Power Sources 194 (2009) 199–205.
[29] J.E. Mink, M.M. Hussain, ACS Nano 7 (2013) 6921–6927.
[30] A. Mehdinia, E. Ziaei, A. Jabbari, Electrochim. Acta 130 (2014) 512–518.
[31] Y.-C. Yong, X.-C. Dong, M.B. Chan-Park, H. Song, P. Chen, ACS Nano 6 (2012) 2394–2400.
[32] Z. He, J. Liu, Y. Qiao, C.M. Li, T.T.Y. Tan, Nano Lett. 12 (2012) 4738–4741.
[33] H. Wang, G. Wang, Y. Ling, F. Qian, Y. Song, X. Lu, S. Chen, Y. Tong, Y. Li, Nanoscale 5 (2013) 10283–10290.
[34] Y. Qiao, X.-S. Wu, C.-X. Ma, H. He, C.M. Li, RSC Adv. 4 (2014) 21788–21793.
[35] H.-T. Chou, H.-J. Lee, C.-Y. Lee, N.-H. Tai, H.-Y. Chang, Bioresour. Technol. 169 (2014) 532–536.
[36] J.E. Mink, J.P. Rojas, B.E. Logan, M.M. Hussain, Nano Lett. 12 (2012) 791–795.
[37] S.K. Smart, A.I. Cassady, G.Q. Lu, D.J. Martin, Carbon 44 (2006) 1034–1047.
[38] T. Sharma, A.L.M. Reddy, T.S. Chandra, S. Ramaprabhu, Int. J. Hydrogen Energy 33 (2008) 6749–6754.
[39] L. Peng, S.J. You, J.Y. Wang, Biosens. Bioelectron. 25 (2010) 1248–1251.
[40] Y. Fan, E. Sharbrough, H. Liu, Environ. Sci. Technol. 42 (2008) 8101–8107.
[41] H. Wang, Z. Wu, A. Plaseied, P. Jenkins, L. Simpson, C. Engtrakul, Z. Ren, J. Power Sources 196 (2011) 7465–7469.
[42] S. Khilari, S. Pandit, M. Ghangrekar, D. Das, D. Pradhan, RSC Adv. 3 (2013) 7902–7911.
[43] H. Ren, H.-S. Lee, J. Chae, Microfluid. Nanofluid. 13 (2012) 353–381.
[44] F. Qian, M. Baum, Q. Gu, D.E. Morse, Lab Chip 9 (2009) 3076–3081.
[45] C.P.B. Siu, M. Chiao, J. Microelectromech. Syst. 17 (2008) 1329–1341.
[46] S. Inoue, E. Parra, A. Higa, Y. Jiang, P. Wang, C.R. Buie, J.D. Coates, L. Lin, Sens. Actuators A Phys. 177 (2012) 30–36.
[47] H. Hou, L. Li, Y. Cho, P. de Figueiredo, A. Han, PLoS One 4 (2009) e6570.
[48] H. Richter, K. McCarthy, K.P. Nevin, J.P. Johnson, V.M. Rotello, D.R. Lovley, Langmuir 24 (2008) 4376–4379.
[49] Z.F. Ren, Z.P. Huang, J.W. Xu, J.H. Wang, P. Bush, M.P. Siegal, P.N. Provencio, Science 282 (1998) 1105–1107.
[50] K.S. Choi, Y.S. Cho, S.Y. Hong, J.B. Park, D.J. Kim, J. Eur. Ceram. Soc. 21 (2001) 2095–2098.
[51] F.S. Gittleson, D.J. Kohn, X. Li, A.D. Taylor, ACS Nano 6 (2012) 3703–3711.
[52] P. Parameswaran, C.I. Torres, H.S. Lee, R. Krajmalnik-Brown, B.E. Rittmann, Biotechnol. Bioeng. 103 (2009) 513–523.
[53] S. Oh, C. Daraio, L.H. Chen, T.R. Pisanic, R.R. Finones, S. Jin, J. Biomed. Mater. Res. Part A 78 (2006) 97–103.
[54] D.-H. Kim, P.P. Provenzano, C.L. Smith, A. Levchenko, J. Cell Biol. 197 (2012) 351–360.
[55] Z. Ren, R.P. Ramasamy, S.R. Cloud-Owen, H. Yan, M.M. Mench, J.M. Regan, Bioresour. Technol. 102 (2011) 416–421.
[56] S. Choi, H.S. Lee, Y. Yang, P. Parameswaran, C.I. Torres, B.E. Rittmann, J. Chae, Lab Chip 11 (2011) 1110–1117.
[57] M. Zurita-Gotor, F.S. Gittleson, A.D. Taylor, J. Blawzdziewicz, Phys. Rev. B 87 (2013) 195449.
[58] J.L. Tan, J. Tien, D.M. Pirone, D.S. Gray, K. Bhadriraju, C.S. Chen, Proc. Natl. Acad. Sci. 100 (2003) 1484–1489.
[59] Z. Ren, H. Yan, W. Wang, M.M. Mench, J.M. Regan, Environ. Sci. Technol. 45 (2011) 2435–2441.
[60] D.Y. Lyon, F. Buret, T.M. Vogel, J.-M. Monier, Bioelectrochemistry 78 (2010) 2–7.
[61] J.S. McLean, G. Wanger, Y.A. Gorby, M. Wainstein, J. McQuaid, S.i. Ishii, O. Bretschger, H. Beyenal, K.H. Nealson, Environ. Sci. Technol. 44 (2010) 2721–2727.
[62] P. Aelterman, W. Verstraete, Trends Biotechnol. 27 (2009) 168–178.
[63] P. Clauwaert, P. Aelterman, L. De Schamphelaire, M. Carballa, K. Rabaey, W. Verstraete, Appl. Microbiol. Biotechnol. 79 (2008) 901–913.
[64] A. ElMekawy, H.M. Hegab, X. Dominguez-Benetton, D. Pant, Bioresour. Technol. 142 (2013) 672–682.
[65] D.R. Bond, S.M. Strycharz-Glaven, L.M. Tender, C.I. Torres, ChemSusChem 5 (2012) 1099–1105.
[66] J. Stevens, SAE Technical Paper 1999-01-2564, 1999, http://dx.doi.org/10.4271/1999-01-2564.
[67] S.J. Roundy, Doctoral Dissertation, University of California, 2003.
[68] R. Vullers, R. van Schaijk, I. Doms, C. Van Hoof, R. Mertens, Solid-State Electron. 53 (2009) 684–693.
[69] M. Seok, S. Hanson, Y.S. Lin, Z. Foo, D. Kim, Y. Lee, N. Liu, D. Sylvester, D. Blaauw, in: IEEE, 2008, pp. 188–189.
[70] M. Hempstead, N. Tripathi, P. Mauro, G.Y. Wei, D. Brooks, in: IEEE, 2005, pp. 208–219.
[71] V. Pillai, H. Heinrich, D. Dieska, P.V. Nikitin, R. Martinez, K.V.S. Rao, IEEE Trans. Circuits Syst. I Reg. Pap. 54 (2007) 1500–1512.
[72] J.C. Biffinger, R. Ray, B. Little, B.R. Ringeisen, Environ. Sci. Technol. 41 (2007) 1444–1449.
[73] D.R. Bond, D.R. Lovley, Appl. Environ. Microbiol. 69 (2003) 1548–1555.
[74] H.J. Kim, H.S. Park, M.S. Hyun, I.S. Chang, M. Kim, B.H. Kim, Enzyme Microb. Technol. 30 (2002) 145–152.
[75] H. Liu, S. Cheng, L. Huang, B.E. Logan, J. Power Sources 179 (2008) 274–279.
[76] Y. Fan, H. Hu, H. Liu, J. Power Sources 171 (2007) 348–354.
[77] M. Chiao, K.B. Lam, L. Lin, J. Micromech. Microeng. 16 (2006) 2547.
[78] T. Shimoyama, S. Komukai, A. Yamazawa, Y. Ueno, B.E. Logan, K. Watanabe, Appl. Microbiol. Biotechnol. 80 (2008) 325–330.